Fuel Processing Technology 247 (2023) 107803

Contents lists available at ScienceDirect

Fuel Processing Technology

journal homepage: www.elsevier.com/locate/fuproc

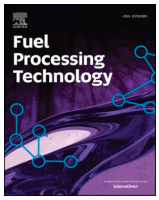

Facile transformation of heavy oil residues into carbon composites used for high-performance supercapacitors

Jessica D. Ortiz-González [a], Ferley A. Vásquez [a], Franky E. Bedoya-Lora [a], Oscar A. Vargas [b], Jorge A. Calderón [a,*]

[a] Centro de Investigación, Innovación y Desarrollo de Materiales – CIDEMAT, Universidad de Antioquia, Cr. 53 No 61 – 30, Torre 2, Lab. 330, Medellín, Colombia
[b] Escuela de Ingeniería Metalúrgica y Ciencia de Materiales, Universidad Industrial de Santander, Carrera 27 Calle 9, Bucaramanga, Colombia

ARTICLE INFO

Keywords:
Asphaltene
Supercapacitor
Activated carbon
Chemical activation

ABSTRACT

Asphaltene, an otherwise undesirable waste from the oil industry, was refined from heavy oil fractions and processed under different conditions to obtain carbonaceous materials with large surface area to be used in supercapacitors. Carbon electrode materials were successfully fabricated by a facile thermal process using melamine foam as template and KOH activation. The effect of different synthesis parameters on morphological and electrochemical performance is reported, namely, the weight ratio KOH:asphaltene, homogenization time, temperature and duration of thermal treatment. The materials were characterized by Raman, BET, SEM/EDS, and XPS; and their performance, in terms of specific capacitance and stability, was assessed by different electrochemical methodologies. Results show that an optimized material, using specific capacitance and active material recovery as optimization targets, was obtained by using a KOH: asphaltene weight ratio of (3:1), homogenization time of 1 h and thermal treatment at 700°C for 0.5 h. This material had a specific energy of 8.6 W h kg^{-1}, specific power of 645 W kg^{-1} and a specific capacitance of 112 F g^{-1} at 0.4 A g^{-1} current density.

1. Introduction

The accelerated growth rate, at which today's society advances, has generated the progressive depletion of natural resources and increased pollution, generating a growing interest in the harvesting of renewable energy sources. However, given the low energy conversion efficiency and the intermittent nature of these sources, the coupling of energy storage systems is required to counteract these effects [1–3]. Hence, there is great interest in the development of materials to be used in electrochemical energy storage devices [4]. Among these materials, supercapacitors and batteries are the main technologies currently deployed at a commercial level. Each of these has a different impact area given their intrinsic characteristics, e.g. vehicle ignition supported by supercapacitors, or portable and stationary energy storage with Li-ion batteries [5,6].

The development of renewable energies must be progressive, based on advances in generation, storage, and distribution technologies [7], thereby allowing a smoother transition away from fossil fuels. Nevertheless, the oil industry will continue to exist in the near future due to the existence of considerable oil reserves, and our dependence on carbon-based products, e.g. organic solvents and polymers [8]. Thus, it is still necessary to seek new products with greater added value derived from, otherwise worthless, heavy fractions. Heavy fractions, usually considered as waste from oil refining processes, are composed of paraffins, resins and asphaltenes, among other by-products [9,10]. Resins and asphaltenes can be useful after heat treatment and chemical activation, which converts them to heteroatom-rich carbonaceous materials with favorable pseudocapacitive characteristics. Additionally, a balance must be achieved between the specific surface area, which gives high capacitance and reversibility, and the surface functional groups, which generate reversible electrochemical reactions for additional energy storage [3,4,11–13].

A key point in the activation process consists of dissolving the base material, e.g. asphaltenes, in aromatic solvents and subsequently adding an activating agent in aqueous solution. This forms an emulsion with both phases. The smaller the microdroplets used, the greater the surface area in the final product [13,14]. In order to maintain a stable emulsion, it is important to embed the mixture in a template during the evaporation of the solvent. Melamine foams are an excellent option for templates, since they are inexpensive and readily available materials that

* Corresponding author.
E-mail address: ANDRES.CALDERON@UDEA.EDU.CO (J.A. Calderón).

https://doi.org/10.1016/j.fuproc.2023.107803
Received 20 November 2022; Received in revised form 18 February 2023; Accepted 22 April 2023
Available online 4 May 2023

are rich in nitrogen groups. They are widely used in activated carbon-based supercapacitors because they can provide a pseudocapacitive character, and also serve as a micro structured template and additional carbon source [15,16].

The materials used in supercapacitors are characterized by having high surface areas. They are also inexpensive and have a low carbon footprint, which allows them to be used in devices that require high power output in short periods. However, since surface interactions do not achieve high energy densities, materials with heteroatom functional groups [17–19] or electrolytes with wider stability windows, e.g. water-in-salt electrolytes, can be sought in order to increase their specific energy densities [20–22].

In this work, a supercapacitor material was synthesized by chemical activation with KOH. The base asphaltene material, derived from Colombian oil, was impregnated in a commercial melamine sponge following a similar procedure reported by Enayat et al. for the active material synthesis process [22]. The effect of variables such as the precursors' homogenization and thermal treatment conditions were investigated. Supercapacitors were built with the synthesized active material and their specific capacitance was evaluated. Additionally, morphological, physicochemical, and electrochemical characterization was performed to determine the effect of the surface functional groups on capacitance and cycling stability. The results showed that the materials had uniform pores, which are characteristic of activated carbons. Imide, carboxyl and ether functional groups were also present, and gave the materials a predominant pseudocapacitive character, which affected the life cycle of the supercapacitor when using an aqueous electrolyte. Finally, it was possible to observe the importance of the homogenization and heat treatment process in obtaining carbonaceous materials with greater surface area and greater presence of surface functional groups.

The process reported in here has been optimized to produce suitable carbon-based materials for supercapacitors. The paper reports a facile and less energy intensive methodology to produce active carbon material, compared to those reported in the literature. Lower quantities of KOH respect to those reported by previous works were used to produce high surface area materials by using cheap and commercially available templates (melamine foam), and otherwise unprofitable heavy fraction byproducts from the oil industry. The variation in functional groups with the thermal treatment temperature was studied in order to evaluate its role in energy capacity and stability performance.

2. Experimental section

2.1. Materials

Solid heavy oil fractions (asphaltene source material) were supplied by a Colombian oil company. The element composition and metal content of raw heavy oil fractions was determined by combustion technique (C, H, N, S) and was carried out in a LECO model CHNS 628 analyzer. The results of that analysis are presented in the Table S1, in the supporting information. Potassium hydroxide flakes (Panreac, 98%) were used as activating agent, recovered n-hexane was used to separate asphaltene from the heavy oil fractions, analytical grade toluene (Panreac, 99.5%) was used as solvent in the activation process and commercial melamine foams were cut into 1 cm cubes and used as templates.

2.2. Asphaltene purification

Ground heavy oil fractions were wrapped in nylon filters (2 μm pore diameter), placed in a thimble, and positioned inside a Soxhlet extractor. Heavy oil fractions were continuously washed with n-hexane (90°C) until the solvent in the thimble compartment was transparent, a process lasting approximately 2 days.

2.3. Asphaltene activation

An experimental design was carried out to find, as far as possible, lower values of the KOH/asphaltene ratios, considering, among other reasons, lower energy consumption, high material recovery and the integrity of the components of the tubular oven, which were found to be affected by high KOH/asphaltene ratios. Hence, 0.6 g of ground and washed asphaltene was dissolved in 36 mL of toluene, to which the required amount of potassium hydroxide of 0.0, 0.6, 1.8 or 3.0 g dissolved in 4.5 mL of deionized water were added to produce KOH/asphaltene ratios of 0.0, 1.0, 3.0 and 5.0, respectively. The solutions were stirred for 1 h at 500 rpm (magnetic or blade stirring). The suspension was obtained by two routes. For the first route, the aqueous solution was added to the asphaltene solution and homogenized with an ultrasonic probe at 130 W for 10 min (Sonics, VCX 130). For the second route the suspension was homogenized for 10 min in an ultrasonic bath (Branson, 1540R-DTH), then further homogenized with a blade stirrer (Caframo, BDC250) at 2500 rpm for 20 or 60 min.

Immediately after the stirring was stopped, 20 pieces (1 cm^3) of melamine sponge were added and evenly soaked with the suspension. The sponges were dried naturally in the fume hood overnight, and further dried for 1 h in a vacuum oven at 90°C. Next, the dried foams were placed in an alumina combustion crucible and subjected to thermal treatment in a tubular oven (Thermo Fisher Scientific, TF55035A-1) under argon atmosphere. The sample was heated for 1 h until the desired temperature was reached (700, 800 or 900°C) and held for 0.5 h.

The samples of active materials obtained from the different KOH/asphaltene ratios were tested and the material with best response to rate-capability, specific capacitance, and recovery percent tests was selected as optimum.

2.4. Activated material washing

The resulting carbon sponges were ground in a mortar and mixed with 1 mL of 1 M HCl for every 100 mg of KOH (added during activation) to neutralize the residual KOH. The powders were placed in an ultrasonic bath for 5 min and subsequently centrifuged at 6000 rpm for 1 h. The supernatant was discarded, and the precipitate was repeatedly washed with an ethanol:acetone mixture (2:1) until the supernatant had a pH close to 7.

2.5. TGA analysis of precursors

The precursors (purified asphaltene, sponge-templated asphaltene and sponge-templated asphaltene + KOH) were characterized by thermogravimetric analysis (TGA) and differential scanning calorimetry (DSC) in argon atmosphere with a heating ramp of 10°C min^{-1} (TA Instruments, SDT Q600) to determine suitable temperatures for the heat treatments.

2.6. Factor analysis to maximize capacitance

With the aim of maximizing the capacitance, the effect of several conditions during the synthesis were assessed: (*i*) amount of KOH added to the solution, (*ii*) homogenization time, (*iii*) thermal treatment temperature and (*iv*) time. The active materials were named as follows: (KOH:Asphaltene weight ratio) – homogenization time in hours – thermal treatment temperature in °C – thermal treatment time in hours.

For the optimization, the selection criteria were (*i*) the specific capacitance measured from cyclic voltammetry between 0.01 and 0.8 V vs. Ag|AgCl at a scanning speed of 10 mV s^{-1}, and (*ii*) the percentage of active material recovered after the centrifugal washing process with respect to the initial 0.6 g of ground and washed asphaltene.

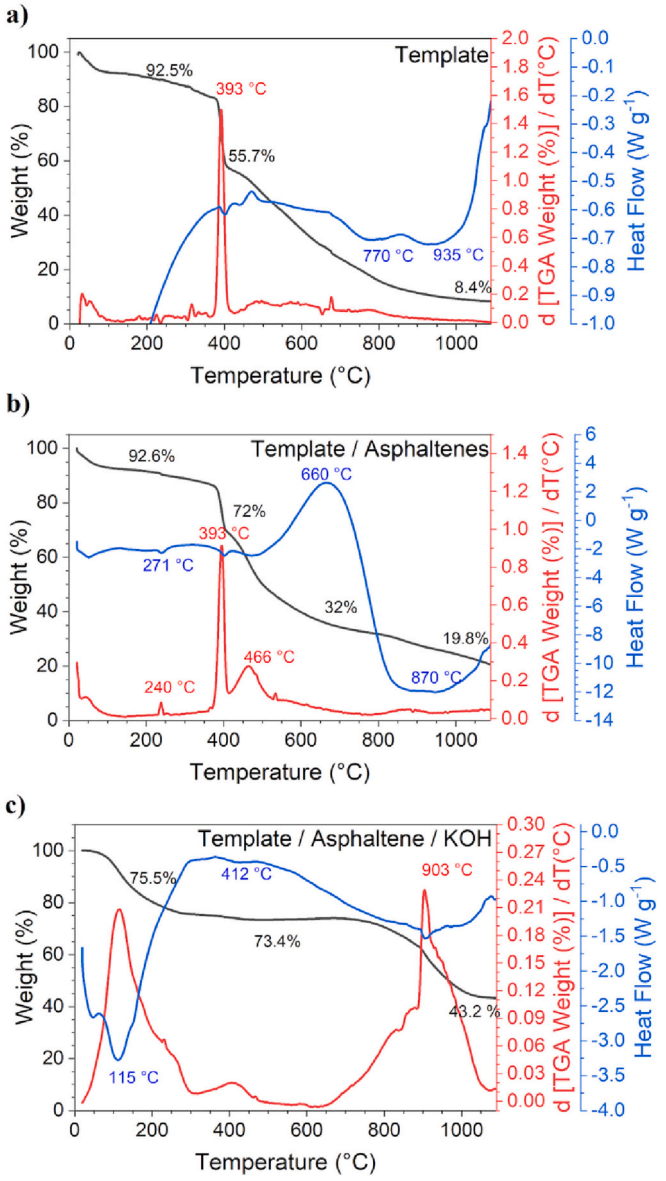

Fig. 1. TGA and DTA measurements under argon atmosphere with a heating rate of 10°C min^{-1}, a) melamine template, b) template and asphaltene and c) template and KOH:Asphaltene ratio of 5:1.

2.7. Supercapacitor device testing

For the fabrication of electrodes to be used in supercapacitors, powders were mixed using a weight ratio of 80:10:10 for active material: carbon Super P: polyvinylidene fluoride binder (PVDF, purchased from Sigma-Aldrich), then suspended in 600 cm^3 *N*-methyl-2-pyrrolidone (NMP, Merck Millipore®) for every 80 mg of active material, and stirred at 1200 rpm for 24 h. The electrodes were prepared by drop, coating the slurry on a previously sandblasted stainless-steel sheet (0.1 mm thickness) and dried in a vacuum oven at 90°C for 24 h.

The electrodes were assessed in two cell configurations. The first of these was a borosilicate beaker with 10 cm^3 of 1 M H_2SO_4 as electrolyte, a steel mesh as counter electrode and Ag|AgCl Sat. KCl (0.197 V vs. SHE) as a reference electrode. This assembly was used for cyclic voltammetry and electrochemical impedance spectroscopy measurements. The second configuration consisted of a T-cell (Swagelok) used as a 2-electrode symmetric cell, both with a similar weight of active material, filled with 400 μL 1 M H_2SO_4 and separated by glass fiber. This assembly was used for rate-capability and stability tests.

2.8. Characterization of sponge-templated, asphaltene-derived carbon electrode materials

The sponge-templated active carbons were characterized by RAMAN spectroscopy (Horiba Jobin Yvon, Nikon BX41) with a laser source of 632 nm. Specific surface area was measured by Brunauer-Emmett-Teller (BET, Micromeritics, ASAP 2020) and the pore size distribution was calculated by Density functional theory (DFT) model with N_2 and CO_2 gas flow. The morphology and elemental composition were studied by scanning electron microscopy (SEM, JEOL JSM 6490LV) coupled to energy scattered X-ray spectroscopy (EDX).

Carbon hydrogen and nitrogen (CHN) analysis (SUNDY, CHN_{435}) and X-ray photoelectron spectroscopy (NAPXPS Specs, Phiobos 150 1D-DLD analyzer) with monochromatic Al-Kα source (1486.7 eV, 13 kV, 100 W) were performed on certain materials (preassemble and post-mortem electrodes) to clarify inconsistencies between the measured areas and effective capacitances.

3. Results and discussion

TGA and DTA analyses were performed, see Fig. 1, to evaluate transitions that took place during thermal treatment and to determine adequate temperature ranges for thermal treatments. The mass loss before 100°C in all materials was due to the physically absorbed water and solvent (toluene). TGA and DTA analyses of melamine sponge template in Fig. 1a show a mass loss of 44.3% and an endothermic peak at 393°C, which corresponds to melamine degradation [23]. At 1100°C the residual mass was 8.4% [23]. The same analysis for the melamine sponge template impregnated with asphaltene is shown in Fig. 1b. This shows a first mass loss of 28% and an endothermic peak at 393°C, also corresponding to melamine degradation [23], and a second mass loss of 20% and endothermic peak at 466°C, corresponding to the degradation of asphaltene to produce coke. Up to 450°C, it is expected that only hydrogen atoms will be lost for the aromatic structure to be built, while keeping heteroatoms such as oxygen, nitrogen, and sulfur [24–26]. The exothermic peak at 660°C corresponds to asphaltene decomposition, which produces a carbonized layer that continues to burn, generating a large amount of heat. The endothermic peaks observed in the range of 800 to 1100°C could be associated with carbon rearrangement, mainly from the source of melamine, and to a lesser extent with the loss of heteroatoms from the asphaltenes [23,26,27]. The residual mass at 1100°C was 19.8%.

TGA and DTA analyses for the melamine sponge template impregnated with asphaltene and activated with KOH (5:1 weight ratio of KOH and asphaltenes) are shown in Fig. 1c. Results show an endothermic peak at 115°C and mass loss between 25 and 300°C (24.5%) corresponding to the release of remanent toluene in the impregnated template. The typical mass loss of 2.1% and endothermic peak at 412°C corresponding to asphaltene degradation [24] was also observed. An additional mass loss of 30.2% and endothermic peak between 500 and 1100°C were observed, which overlay the various stages of chemical activation and the release of OH^- from KOH [28]. Additionally, up to 800°C, the loss of functional groups associated with the burn-off and release of OH^- from KOH (maximum 18.3% associated with mass loss of OH^-) at elevated temperatures was observed. The loss of functional groups is known to damage the skeleton of the carbonaceous structure, and decrease both the degree of graphitization of the material, as can be seen further in Fig. 3, and the content of functional groups composed of heteroatoms [29,30]. According to TGA results of Fig. 1c the remanent mass after heating at 1100°C corresponds to 43.2%, from which the remanent mass of potassium was calculated as 42.0 wt% respect to the initial mass of the sample (Template/Asphaltenes/KOH; KOH:Asphaltene ratio of 5:1). The procedure used to perform this calculation is described in the supporting information. While the extra 1.2% of

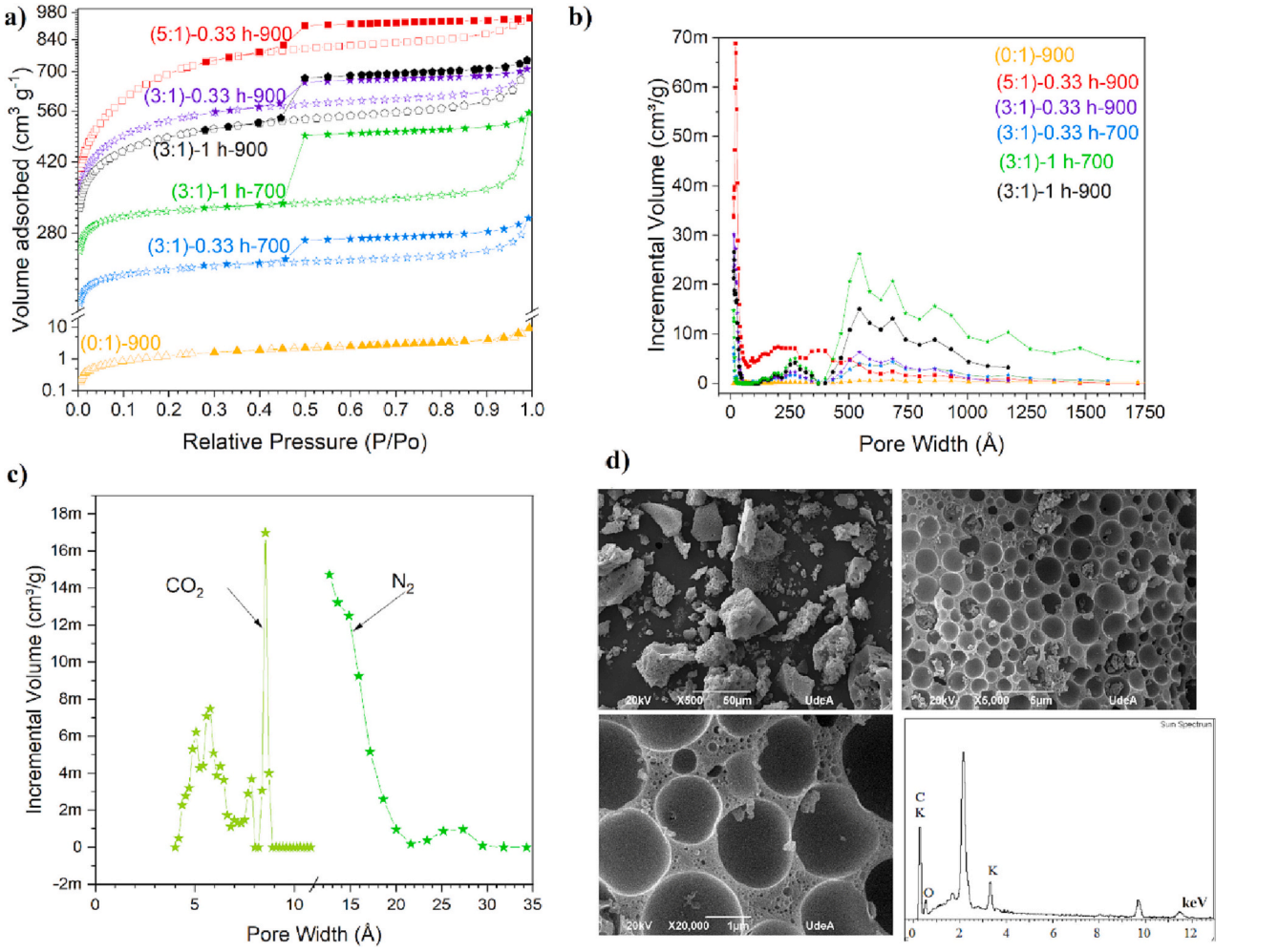

Fig. 2. a) N_2 adsorption isotherms for activated carbon synthesized with KOH:Asphaltene weight ratios of (5:1) and (3:1), blade stirrer homogenization for 0.33 and 1 h and thermal treatment temperature at 700 and 900°C. b) Pore size distribution c) pore size distribution with N_2 and CO_2 of the sample (3:1)-0.33 h-700-0.5 h. d) SEM images of the sample (3:1)-0.33 h-700-0.5 h.

Table 1
Brunauer-Emmett-Teller (BET) specific surface area.

(KOH:Asphaltene) – homogenization time / h – Thermal treatment temperature /°C	S_{BET} /m^2 g^{-1}	$V_{mic} \lessapprox 2$ nm /cm^3 g^{-1}	V_{tot} /cm^3 g^{-1}
(5:1)-0.33 h-900	2264.6	0.375	1.246
(3:1)-0.33 h-900	1501.3	0.375	0.768
(3:1)-0.33 h-700	676.3	0.254	0.342
(3:1)-1 h-900	1650.0	0.400	0.777
(3:1)-1 h-700	942.5	0.334	0.661

S_{BET} – BET specific surface area, V_{tot} – total pore volume, V_{mic} – micropore volume.

remanent mass corresponds to activated porous carbon. It is worth noting that the percentage of remanent mass increased after adding the different compounds to the melamine foam, from 8.4% to 19.8% after adding asphaltene alone, and from 8.4% to 43.2% after adding asphaltene and KOH. This is due noncombustible fraction which remains even after heating at 1000°C.

Surface area, pore size and distribution of active materials after thermal treatment were evaluated by N_2 adsorption isotherms and SEM. Fig. 2a shows the N_2 adsorption-desorption isotherms for some synthesized materials. The results show type IV isotherms characterized by the presence of mesopores, in which the capillary condensation effect is evident. The shape (hysteresis loop 4 according to IUPAC classification) could be associated with hemicylindrical pores, which are characteristic of activated carbons with pore size distribution mainly in micro and nano scale [31,32]. Fig. 2b shows the pore size distribution of the materials. Here, it can be observed that the pore distribution shifts towards lower values with the addition of the activating agent (KOH). It is also observed that the increase in temperature has a two-fold effect, increasing the global surface area, and decreasing the pore sizes. Finally, an increase in the homogenization time (from 20 to 60 min) increased the number of mesopores, which could be associated with hierarchical pore distributions with the presence of micropores, mesopores and macropores [28,33,34]. SEM images and pore distribution in Fig. 2c and d show the presence of meso and macropores homogeneously distributed in the activated carbon obtained with a KOH:asphaltene ratio of (3:1), homogenization time of 1 h, and thermal treatment at 700°C.

The surface areas and pore volume reported in Table 1 are evidence of a prominent effect of temperature, KOH content and, to a lesser degree, the effect of homogenization time, on the surface area. It was observed that as the KOH content increased, the collapse of small-sized micropores was less controlled; an increase in temperature during heat treatment promoted the appearance of micropores and their subsequent collapse, this might be due to the evaporation of potassium metal at high temperatures. On the other hand, the size of the pores increased with homogenization time, and produced the hierarchical structure.

The synthesized materials, as shown in the SEM images of Fig. 2d,

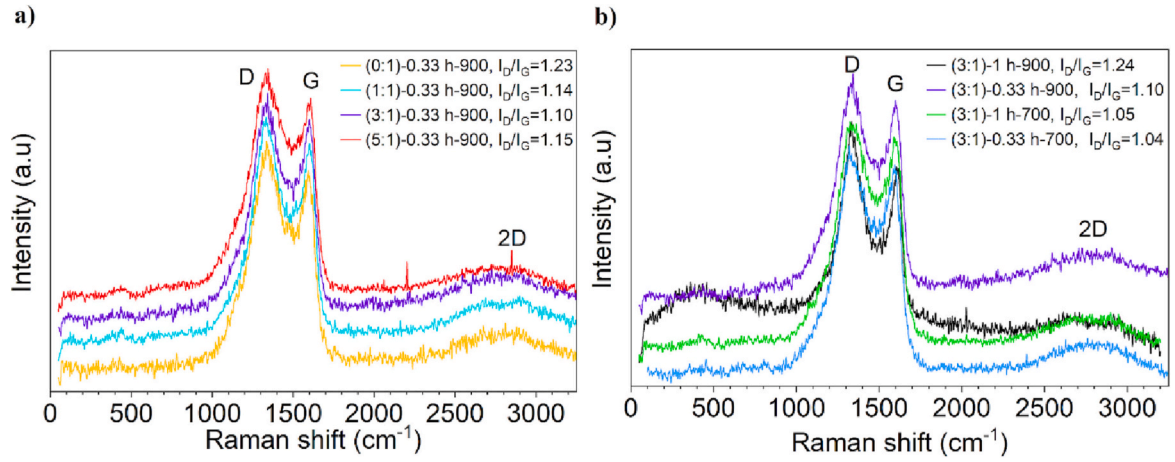

Fig. 3. Raman spectra of synthesized samples under different conditions. (a) Effect of the KOH:Asphaltene weight ratio and (b) homogenization time and thermal treatment temperature on the degree of graphitization.

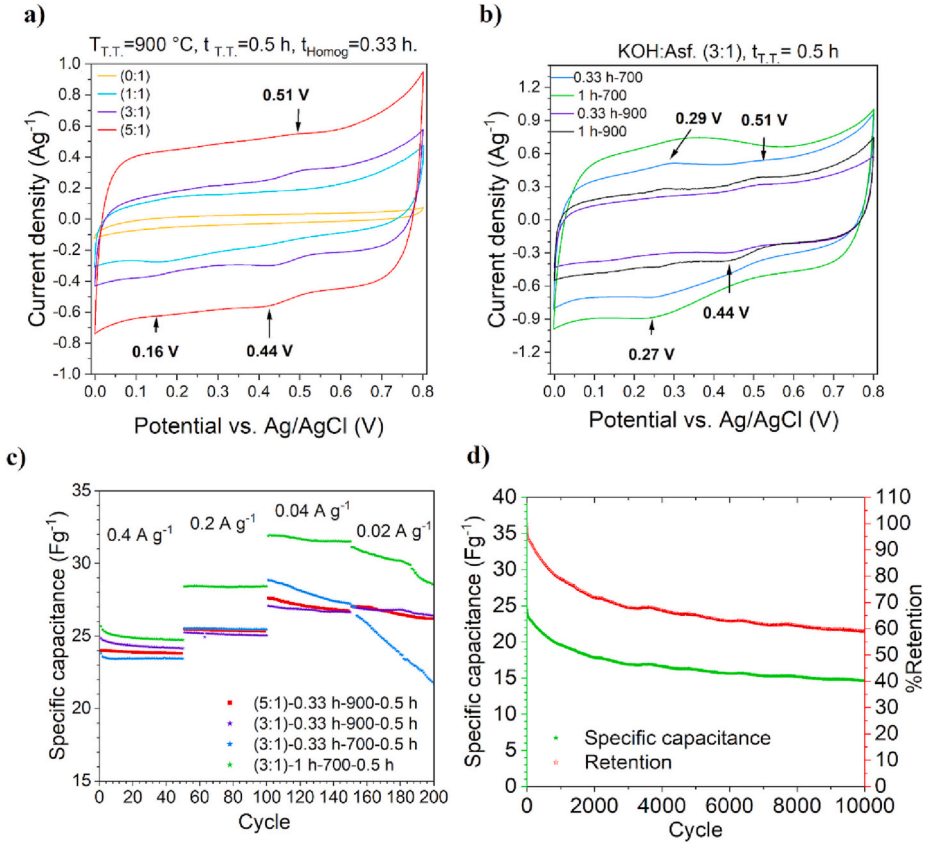

Fig. 4. Cyclic voltammograms of the active materials at 5 mV s^{-1} a) with different KOH:Asphaltene weight ratios and b) different homogenization time (h) – temperatures (°C), c) Rate-capability of some samples and d) Specific capacitance during stability tests at 0.4 A g^{-1} for (3:1)-1 h-700-0.5 h sample.

exhibited a honeycomb-like structure, with spherical macropores of 1.8 ± 0.4 μm and mesopores of 63.9 ± 18.9 nm located between the walls of the macropores. These mesopores were possibly connected by micropores according to the pore distribution [22]. On the other hand, the material obtained without the melamine template (Fig. S1 in the supporting information) exhibited irregular macropores of 5.7 ± 1.7 μm connected by mesopores of 90.5 ± 30.9 nm. In the current case, having a lower proportion of KOH than in previous works reported in the literature, allowed the spherical structures of melamine template to be maintained, while making the macropores to be interconnected through micropores. The melamine template improved the contact area between the carbonaceous material, while the activating agent (KOH) helped to obtain a higher number of micropores and a homogeneous distribution of micro and mesopores. As will be demonstrated below, melamine template improves the mechanical properties of the active material, preventing its collapse during the charge-discharge cycles.

The degree of graphitization, associated with the I_D/I_G ratio, was analyzed by Raman spectroscopy with corresponding spectra shown in Fig. 3. The typical carbon bands, D and G, appear at around 1350 cm^{-1} and 1520 cm^{-1}, respectively. These are associated with amorphous carbon (D) and graphite carbon (G). The D-band derives from disorder in the sp^2-hybridized carbon, while the G-band is related to the tangential

Table 2
Capacitance reports of some carbonaceous materials used as active material in supercapacitors with 1 M H_2SO_4.

Material	Specific Capacitance (F g^{-1})	Ref.
Heavy oil fractions and sponge templated carbon	122	This work
Oil crude and sponge templated carbon	115	[22]
N-rich composite of CNTs and carbon derived from melamine	167	[56]
Onion-like carbon	30	[57]
Quinone-coated onion-like carbon	264	[57]
Nitrogen-rich cocoon silk derived carbon	392	[58]
N/O/S-doped hierarchical porous carbon materials	549	[59]

stretching (E_{2g}) mode of graphite [35–37]. The broad-2D band at approximately 2700 cm^{-1} is related to the second order Raman scattering process [35,38]. The activation with KOH slightly promoted graphitization, and no significant difference was observed with increasing KOH at 900°C. On the other hand, increasing temperature during the thermal treatment increases the I_D/I_G ratio (lower graphitization); hence, the highest degree of graphitization was obtained for the materials treated at 700°C. Similarly, the increase in the heat treatment time increased the I_D/I_G ratio, although a lesser effect was observed at 700°C [39]. These results suggest that the mass loss at elevated temperatures (>650°C) affect the functional groups and the skeleton of the carbonaceous structure, as was observed in the TGA analysis in Fig. 1c.

Cyclic voltammetry tests and charge-discharge cycles were performed to evaluate the capacitance and stability of the active materials. Cyclic voltammograms in Fig. 4a, performed on active materials with different KOH:Asphaltene weight ratios, show anodic peaks at 0.51 V vs. Ag|AgCl and cathodic peaks at 0.44 and 0.16 V vs. Ag|AgCl. The faradaic process at 0.44 and 0.51 V increased with the amount of KOH. Fig. 4b shows the CV curves performed for materials prepared with various homogenization times and temperatures. Anodic peaks at 0.29 and 0.51 V vs. Ag|AgCl, and cathodic peaks at 0.44 and 0.27 V vs. Ag|AgCl are observed. The faradaic processes at 0.27 and 0.29 V could be associated with the reversible reaction found in activated carbons rich in nitrogen groups [40]. High intensities for the materials thermally treated at 700°C were observed. The faradaic processes at 0.44 and 0.51 V are associated with reactions of carboxylic groups such as quinone/hydroquinone redox couple [40–42]. High intensities for the materials thermally treated at 900°C were observed. Additionally, cyclic voltammograms in Fig. 4b shows a higher faradaic effect with increasing homogenization time. The capacitance values (shown further in Table 3) increase with increased amount of KOH and homogenization time. This is due to the increase in the BET area and to the hierarchical structure, which facilitates the entry of ions into the structure [33,43,44]. The materials thermally treated at 700°C exhibited a lower specific surface

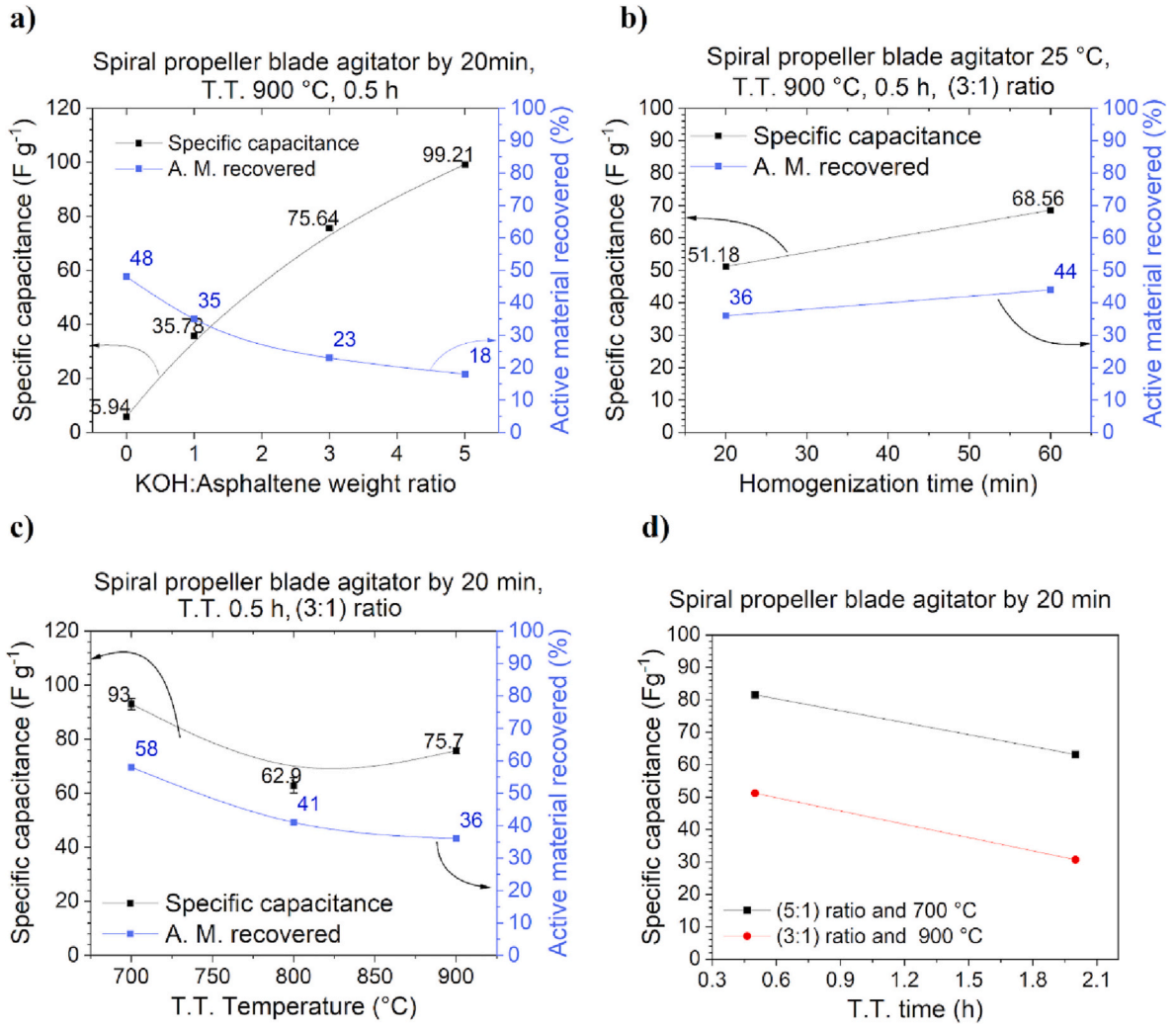

Fig. 5. Specific capacitance response and active material recovered percentage after the washing process for synthesis under different conditions. Effect of a) the amount of KOH, b) homogenization time, c) heat treatment temperature and d) heat treatment time.

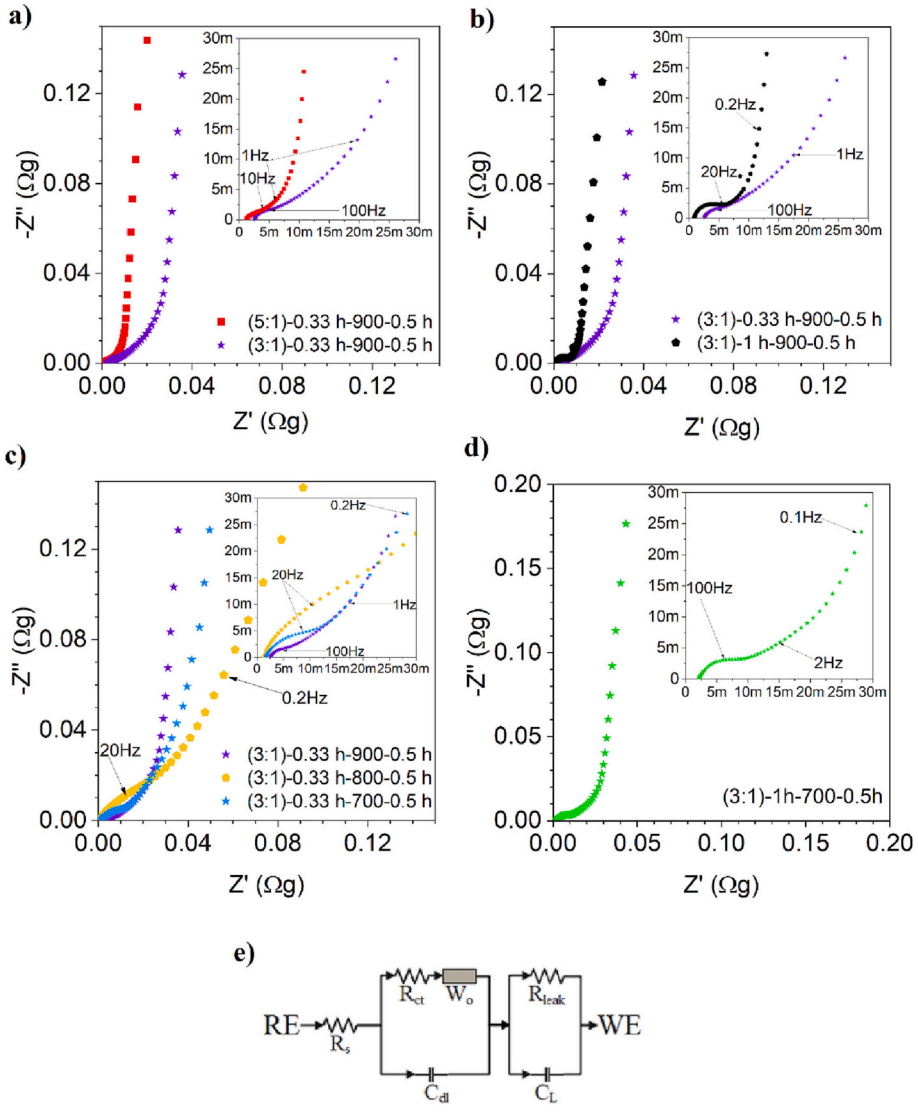

Fig. 6. Nyquist diagrams of supercapacitors in 1 M H_2SO_4. a) Effect of the amount of KOH added, b) effect of homogenization time, c) effect of heat treatment temperature, d) spectra of the material with highest capacitance: KOH:Asphaltene (3:1) and e) equivalent circuit used in the analysis of electrochemical impedance spectra.

Table 3
Parameters calculated by equivalent circuit fitting of electrochemical impedance spectra for different supercapacitors synthesized at different conditions: KOH: Asphaltene ratio, homogenization time and thermal treatment temperature.

Active material	R_s	R_1	C_1	W_1	R_2	C_2 (EIS)	C_2 (5mHz)	C_2 (CV/ 10 mV s^{-1})	C_2 (Cycling/ 0.4 A g^{-1})
	Ω g	Ω g	F g^{-1}	MΩ g^{-1}	Ω g	F g^{-1}	F g^{-1}	F g^{-1}	F g^{-1}
(3:1)-1 h-700-0.5 h	0.0021	0.01	0.106	45	0.958	92.7	90.28	123	112
(3:1)-0.33 h-900-0.5 h	0.0024	0.008	0.117	39.1	1.274	80.21	80.17	86	84
(3:1)-0.33 h-700-0.5 h	0.0016	0.01	0.236	31.1	2.625	56.92	52.96	94	92
(3:1)-0.33 h-800-0.5 h	0.0013	0.023	0.186	12.7	3.564	25.23	19.17	70	56
(5:1)-0.33 h-900-0.5 h	0.0011	0.005	0.656	104	2.045	84.6	90.06	100	96

Table 4
Global elemental analysis using CHN of samples before and after thermal treatment.

Sample	% C	% H	% N	%O	% Ash
Untreated	86.68	7.83	1.93	2.81	0.45
700°C	70.38	2.97	2.27	14.62	9.76
900°C	87.08	1.90	1.69	5.52	3.81

area than those treated at 900°C; however, the faradaic processes at 0.37 and 0.29 V in the material treated at 700°C increased due to the presence of functional groups on the surface [45], which were still present in higher concentrations when treated at lower temperature. This will be confirmed later by elemental CHN analysis and XPS in Tables 4 and 5. Hence, as can be seen in Fig. 4d, the balance between the specific surface area and the number of functional groups improved the specific capacitance [46,47]. On the other hand, cyclic voltammetry results of the

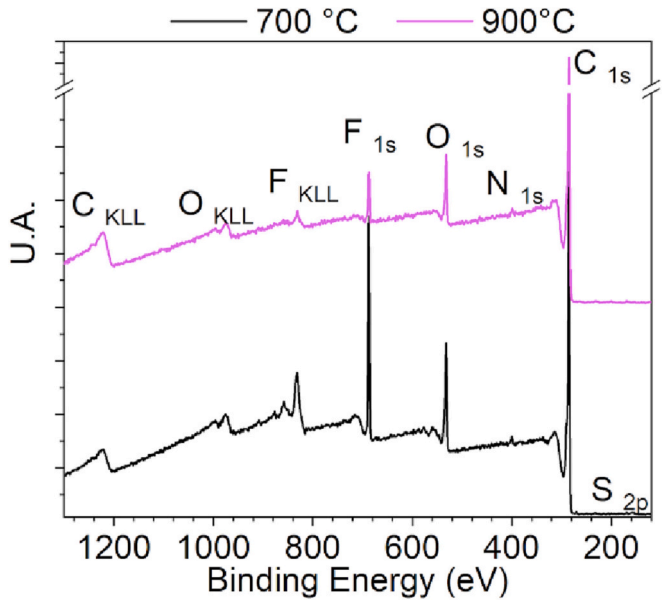

Fig. 7. XPS survey spectra of the activated carbon electrodes obtained at 700°C and 900°C, 1 eV step.

Table 5
Surface elemental analysis from XPS spectra.

Element	Position (eV)	700°C pre-assembly	900°C pre-assembly	700°C post-mortem-Cathode	700°C post-mortem-Anode
		At (%)	At (%)	At (%)	At (%)
C	284.61	89.84	94.61	90.86	89.73
O	532.61	9.39	4.89	7.29	8.58
N	399.61	0.77	0.51	1.53	1.33
S	168.61	–	–	0.32	0.33

(3:1)-1 h-700-0.5 h sample with and without the sponge template, see Fig. S2 in the supporting information, indicate small specific surface area associated with collapse of micropores. Regarding the peaks associated with oxygenated and nitrogenous groups, they are practically undetectable by this technique, showing a low content of O and N, due to the lack of the template material.

Galvanostatic charge-discharge analyses performed on samples at several C-rates, as shown in Fig. 4c, Figs. S3 and S4 (in the supporting information), revealed good stability for most materials. This is consistent with the cyclic voltammetry results. The self-discharge process typical in electrochemical capacitors was observed only when low current densities of 0.02 A g^{-1} were used during the discharge process, but a greater effect was observed in materials with higher percentage of small-sized micropores (especially materials heat-treated at 700°C), since the ion transport rate is controlling the charge transfer at high charge rates [48]. Additionally, the active material with the highest capacitance values ((3:1)-1 h-700-0.5 h) was subjected to a longer stability test, in which a rapid drop in the specific capacitance was observed in the first 2000 cycles (Fig. 4d). This capacitance drop could be associated with the change of functional groups during cycling tests. Equivalent results have been reported by other authors for materials with a high amount of C–O bonds and tested in H_2SO_4 electrolytes [49,50]. The change in the functional groups was confirmed by postmortem XPS analysis, as will be shown below.

The stability can be improved by changing the electrolyte of the supercapacitor [51,52], or by including stabilizing agents during the synthesis [53]. In the case of the material reported in here, additional tests with "water in salt" electrolyte showed high stability; Xi Li et al. reported high stability of porous carbon with functional groups in 1 M KOH electrolyte in which the functional groups were not desorbed; although current collectors need to be carefully evaluated due to impending corrosion [54]. Another option to improve the stability of the supercapacitor is to use a material with lower initial capacitance but having a higher pure capacitive input, i.e., larger micropores that improve the transport of ions towards the surface of the active material providing stability during long cycling.

The symmetric supercapacitor exhibited a specific energy of 8.6 W h kg^{-1} and a specific power of 645 W kg^{-1} (calculated using the methodology presented in the supporting information). These values place the device successfully in the typical range for a supercapacitor/double-layer capacitor, according to the ranges reported by Zhao et al [55] Additionally, the magnitude of the capacitance obtained with the carbonaceous material presented in this work reaches a value that lies in an acceptable range according to literature reports, as can be seen in Table 2, since no additional procedures were used in this work to incorporate heteroatoms that provide its pseudocapacitive character.

Specific capacitances were calculated from cyclic voltammograms to assess the effect of different synthesis parameters and the correlation between capacitance, surface area and functional groups. Fig. 5 summarizes the effect of KOH amount, homogenization time, thermal treatment temperature and time on the specific capacitance and amount of recovered material. Although the increase in KOH improved the specific capacitances, the amount of material recovered after the synthesis decreased. This phenomenon was observed to a lesser extent if the system was stirred only with ultrasound, (Fig. S5 in the supporting information), but as larger emulsion droplet sizes were obtained, it was not possible to achieve sufficient specific surface area, so it was decided to vary the homogenization conditions in an overhead stirrer (it achieves a higher stirring speed) to maximize the contact between the aqueous and organic phases. Longer homogenization times improved capacitance and had no significant effect on the amount of material recovered. The decrease in thermal treatment temperature and time improved the specific capacitance and the recovery of active material. The increases in capacitance with KOH amount and homogenization time are due to the increased number of micro-drops, which enhance the activation effect and the specific surface area, as reported in Table 1. With regard to the amount of recovered material, it was observed that, with increased BET area, less material was recovered, because the smaller particle size promoted the entraining of the material during the subsequent processes of heat treatment, washing and final drying. Hence, the amount of material recovered after the synthesis was designated as an important selection criterion, given the difficulties of handling and material costs associated with the production process of active material for supercapacitors.

Electrochemical impedance spectroscopy (EIS) was used to compare the capacitance values of active materials in 1 M H_2SO_4 electrolyte. Nyquist diagrams of EIS for the different materials are presented in the Fig. 6. Three time-constant equivalent circuit ($[R_s ([R_1W] Q_1) (R_2Q_2)]$), comprising several processes in the electrochemical response, was used to fit the spectra [60]. Process $(RQ)_1$ is related to the charge transfer at the working electrode outer surface, and process $(RQ)_2$ is associated with the capacitance inside the porous electrode (Fig. 6e) [60,61]. W is related to the diffusion process of electroactive species. The capacitive elements were replaced by Constant Phase Elements (CPE, Q) for better fitting. The effective capacities (C_1 and C_2) were calculated from the CPEs following the Brug equation [62]. Table 3 reports the capacitance values found by EIS, cyclic voltammetry at 10 mV s^{-1}, charge-discharge cycling at 0.4 A g^{-1} current density, and by direct calculation of capacitance at 5 mHz using the equation $C = -1/\omega Z''$ [60]. A good agreement between the methods used to calculate the capacitance values was found.

Table 3 shows that, regardless of the capacitance estimation method, the effective capacitance increases with the amount of KOH and homogenization time. This is because of the expected increase in the

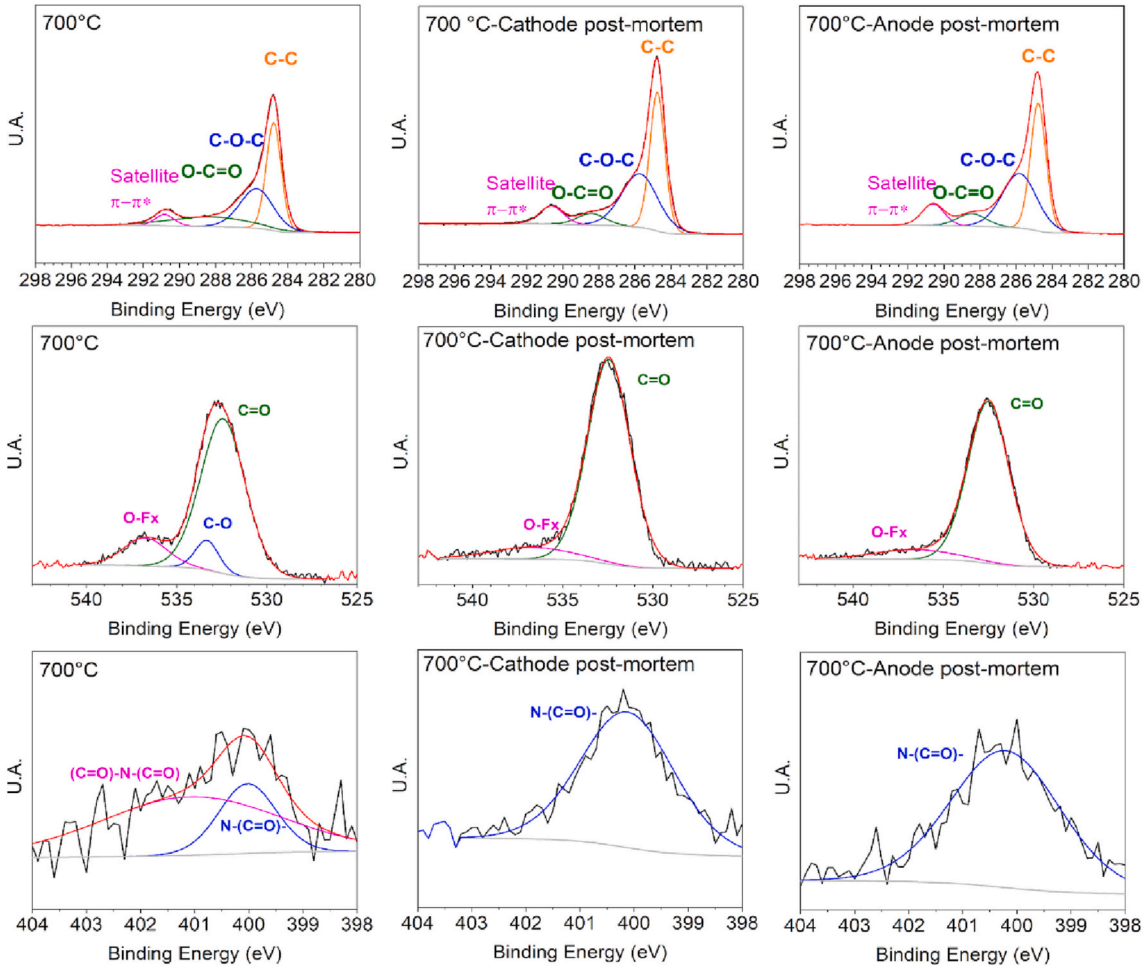

Fig. 8. High-resolution XPS spectra and respective deconvolutions, for pre and post operation electrodes used in a supercapacitor with 1 M H_2SO_4 electrolyte.

Table 6
Elemental composition from XPS analysis of electrodes for pre and post operation in a supercapacitor after 10,000 cycles with current density of 0.4 A g^{-1}.

Valence band	Bonds	700°C pre-assembly (%)	900°C pre-assembly (%)	700°C post-mortem-Cathode (%)	700°C post-mortem-Anode (%)
C_{1s}	C–C	43.43	48.45	47.83	46.84
	C–O–C	35.62	28.92	44.77	44.70
	O–C=O	20.95	22.63	7.41	8.46
O_{1s}	C=O	78.31	76.5	89.96	89.26
	C–O	7.9	4.79	–	–
	O–Fx	13.79	18.71	10.04	10.74
N_{1s}	N–(C=O)	23.51	84.49	100	100
	(C=O)–N–(C=O)	76.49	15.51	0	0

specific surface area. Decreasing the heat treatment temperature to 700°C for the KOH:Asphaltene ratio (3:1) increased the effective capacitance, possibly due to a synergetic effect between the increase in the specific surface area and the enhancement of activity due to the presence of heteroatoms on the surface (pseudocapacitance), which were in higher proportion for low temperature heat treatments. However, a balance must be achieved between the amount of surface functional groups and the electrochemically active area for this effect to occur. For example, the synergetic effect was not observed for temperatures of 800°C and KOH:Asphaltene ratios of (3:1) as seen in Fig. 5c, or for 700°C and the ratio (5:1), Fig. 5d.

The results of CHN elemental analyses of active materials with a KOH:Asphaltene ratio of (3:1), 1 h of homogenization and thermal treatment at 700°C and 900°C, are shown in Table 4. It can be observed that an increase in the thermal treatment temperature decreased the global content of heteroatoms in the material, corroborating that the endothermic peak up to 800°C in the thermogravimetric analysis was associated with the loss of heteroatoms due to the burn-off effect (Fig. 1).

The XPS spectra of electrodes made with materials activated with a KOH:Asphaltene ratio (3:1) are presented in Fig. 7. Expected signals associated with nitrogen, sulfur, carbon, and oxygen were observed: N_{1s}, S_{2p}, C_{1s} and O_{1s} [63,64].This also confirms the findings described before in CHN elemental analysis. Fluorine signals are related to the binder (PVDF). The results show that the content of nitrogen and oxygenated groups on the material surface decrease with increased thermal treatment temperature, as observed in Table 5. XPS high resolution spectra for those regions can be found in the supporting information, Fig. S6. Post-mortem XPS confirms a loss of oxygen groups both in the cathode and in the anode, while the content of nitrogen groups on the surface increased after the stability test (Table 5 and Fig. S7 in the supporting information). This effect may be associated with the breakdown of functional groups integrated in the carbonaceous network. This breakage probably increases the specific surface area and exposes functional groups in the bulk of the carbonaceous material, possibly with melamine origin, where a higher content of functional groups could be found [15].

The high-resolution spectra for N_{1s}, C_{1s} and O_{1s} regions were also

reported, and their respective deconvolutions are presented in Fig. 8 and Table 6. These results show that the materials are composed of surface functional groups of the carboxylic, hydroxyl, ether, ester, quinone, amide, lactam and imids types [40], in addition to the satellite band "shake-up" π−π* associated with delocalization of charges present in aromatic structures [65]. At increased heat treatment temperatures, the proportion of oxygen and nitrogen in the form of heteroatom incorporated in the carbonaceous network decreased, while the proportion of derivatives of carboxylic groups increased, explaining the larger surface area [39]. Regarding the post-mortem results, it is observed that, after the operation of the device, the imide groups are desorbed from the surface, which affects the number of surface defects on the carbonaceous material while increasing the area with ageing. Carboxylic groups also decreased, as observed in the cyclic voltammetry results, where part of the redox couple give the device a pseudocapacitive character. These are the main reasons for the decrease in the capacitance during the stability test of the supercapacitor when assessed in 1 M H_2SO_4 electrolyte (Fig. 4d).

Similarly, the highest specific capacitance values were found for the material thermally treated at 700°C, since the large percentage of heteroatoms on the surface compensates for the lower specific surface area observed in this active material. Despite the large capacitance values observed at initial cycles, the specific capacitance decreased during cycling due to: *(i)* the surface area is composed of a high percentage of small micropores, which with prolonged cycling at a high charge rate can cause the collapse of the structure and reduce the capacitance by loss of surface area, *(ii)* the loss of oxygen and carboxylic functional groups without the hydroxyl groups produced in the reversible electrochemical reactions, and *(iii)* the modification of the nitrogenous functional groups associated with the reduction peak at ~0.27 V vs. Ag|AgCl [40]. For this reason, it is desirable to increase the specific surface area, possibly with better homogenization [22], in order to maintain a stable specific capacitance at an acceptable value, given that after 2000 charge-discharge cycles a significant drop in the specific capacitance was observed (Fig. 4d).

4. Conclusions

The optimized methodology proposed in this study allows for a simple synthesis of materials for supercapacitor devices, by using readily available raw materials and waste from the oil industry. Thermal treatment and KOH concentration were optimized in order to minimize energy requirements, homogenization time, and product losses, while conforming with suitable properties for supercapacitor applications.

Morphological and electrochemical analyses confirmed that an activated carbon synthesized from Colombian heavy oil fractions achieved a better specific surface area, morphology and improved supercapacitor performance when using a commercial melamine foam template. It was also demonstrated that the homogenization of the emulsion of the carbon source and the activating agent is one of the main factors in increasing the specific surface area. In this regard, it was of interest to use high stirring speeds to achieve smaller microdroplets or to increase the homogenization time to obtain a hierarchical architecture.

Additionally, it was found that, for heat treatment at temperatures higher than 800°C, a breakdown of the carbonaceous structure occurs, resulting in a decrease in the degree of graphitization and the content of functional groups composed of heteroatoms. The presence of these functional groups, with melamine or asphaltene origin, can provide desirable pseudo-capacitive behavior. The optimized material, thermally treated at 700°C and 1 h of homogenization time, achieved an energy density of 8.6 W h kg^{-1} and a specific capacitance of 112 F g^{-1} at 0.4 A g^{-1} current density. The stability of the materials depended mainly on the stability of the oxygen and nitrogen-containing functional groups, since the decrease in the Faradaic character caused a decrease in the specific capacitance with the ageing of the device, as was observed for the optimized material obtained with a KOH:Asphaltene weight ratio of (3:1), homogenized for 1 h and thermally treated at 700°C for 0.5 h.

CRediT authorship contribution statement

Jessica D. Ortiz-González: Investigation, Formal analysis, Writing - original draft. **Ferley A. Vásquez:** Investigation, Formal analysis, Methodology, Writing - original draft. **Franky E. Bedoya-Lora:** Investigation, Conceptualization, Formal analysis, Writing - original draft. **Oscar A. Vargas:** Formal analysis, Validation. **Jorge A. Calderón:** Conceptualization, Methodology, Formal analysis, Project administration, Resources, Writing - review & editing.

Declaration of Competing Interest

The authors declare that they have no known competing financial interests or personal relationships that could have appeared to influence the work reported in this paper.

Data availability statement

Data available on request from the interested.

Acknowledgment

The authors acknowledge the financial support by Ecopetrol S.A. and UNIRED through the InnóvaTe 2020 project, and the help of Dr. Jennifer Laverde for the BET area measurements.

Appendix B. Supplementary data

See in supplementary information: SEM images of the optimal carbon without sponge template; Electrochemical calculations for specific capacitance; Cyclic voltammetry of the sample with and without the sponge template; Rate-capability measurements at different conditions; Load profiles; Effect of the KOH/Asphaltene ratio on the specific capacitance; XPS survey electrodes spectra and High-resolution XPS spectra of the material activated at different conditions; References. Supplementary data to this article can be found online at https://doi.org/10.1016/j.fuproc.2023.107803.

References

[1] P. Li, Energy storage is the core of renewable energy technologies, IEEE Nanotechnol. Mag. 2 (4) (2008) 13–18, https://doi.org/10.1109/MNANO.2009.932032.
[2] R. Zahedi, M.M. Ardehali, Power management for storage mechanisms including battery, supercapacitor, and hydrogen of autonomous hybrid green power system utilizing multiple optimally-designed fuzzy logic controllers, Energy 204 (2020) 117935, https://doi.org/10.1016/j.energy.2020.117935.
[3] Jana, A.; Paul, R.; Roy, A. K. Chapter 2 - Architectural design and promises of carbon materials for energy conversion and storage: in laboratory and industry. In *Micro and Nano Technologies*; Paul, R., Etacheri, V., Wang, Y., Lin, C.-T. B. T.-C. B. N. for A. T. and E. E. S. and C, Eds.; Elsevier, 2019; pp. 25–61. https://doi.org/10.1016/B978-0-12-814083-3.00002-0.
[4] H. Hu, M. Wu, Heavy oil-derived carbon for energy storage applications, J. Mater. Chem. A 8 (15) (2020) 7066–7082, https://doi.org/10.1039/d0ta00095g.
[5] M. Winter, R.J. Brodd, What are batteries, fuel cells, and supercapacitors? Chem. Rev. 104 (10) (2004) 4245–4270, https://doi.org/10.1021/cr020730k.
[6] N. Gyawali, Y. Ohsawa, Integrating fuel cell/electrolyzer/ultracapacitor system into a stand-alone microhydro plant, Energy Convers. IEEE Trans. 25 (2011) 1092–1101, https://doi.org/10.1109/TEC.2010.2066977.
[7] M. Seckin Salvarli, H. Salvarli, For Sustainable Development: Future Trends in Renewable Energy and Enabling Technologies, *Intech*, , https://doi.org/10.5772/intechopen.91842 *i* (tourism), 13.
[8] International Energy Agency, The Future of Petrochemicals – Analysis, Int. Energy Agency, 2018, pp. 11–25.
[9] M. Kamkar, G. Natale, A review on novel applications of asphaltenes: a valuable waste, Fuel 2021 (285) (September 2020) 119272, https://doi.org/10.1016/j.fuel.2020.119272.
[10] R. Marappa Gounder, Introductory Chapter: Heavy Crude Oil Processing - An Overview, Intech, 2016 (i (tourism), 13).
[11] Z. Abedi, D. Leistenschneider, W. Chen, D.G. Ivey, Superior performance of electrochemical double layer supercapacitor made with asphaltene derived

activated carbon fibers, Energy Technol. 8 (12) (2020), https://doi.org/10.1002/ente.202000588.
[12] F. Qin, X. Tian, Z. Guo, W. Shen, Asphaltene-based porous carbon nanosheet as electrode for supercapacitor, ACS Sustain. Chem. Eng. 6 (11) (2018) 15708–15719, https://doi.org/10.1021/acssuschemeng.8b04227.
[13] J. Wang, S. Kaskel, KOH activation of carbon-based materials for energy storage, J. Mater. Chem. 22 (45) (2012) 23710–23725, https://doi.org/10.1039/c2jm34066f.
[14] M. Sevilla, N. Díez, A.B. Fuertes, More sustainable chemical activation strategies for the production of porous carbons, ChemSusChem 14 (1) (2021) 94–117, https://doi.org/10.1002/cssc.202001838.
[15] Y. Shi, G. Liu, R. Jin, H. Xu, Q. Wang, S. Gao, Carbon materials from melamine sponges for supercapacitors and lithium battery electrode materials: a review, Carbon Energy 1 (2) (2019) 253–275, https://doi.org/10.1002/cey2.19.
[16] R. Zhang, X. Jing, Y. Chu, L. Wang, W. Kang, D. Wei, H. Li, S. Xiong, Nitrogen/oxygen co-doped monolithic carbon electrodes derived from melamine foam for high-performance supercapacitors, J. Mater. Chem. A 6 (36) (2018) 17730–17739, https://doi.org/10.1039/c8ta06471g.
[17] S. Zhang, X. Shi, X. Chen, D. Zhang, X. Liu, Z. Zhang, P.K. Chu, T. Tang, E. Mijowska, Large-scale and low-cost motivation of nitrogen-doped commercial activated carbon for high-energy-density supercapacitor, ACS Appl. Energy Mater. 2 (6) (2019) 4234–4243, https://doi.org/10.1021/acsaem.9b00481.
[18] L. Yu, G.Z. Chen, Supercapatteries as high-performance electrochemical energy storage devices, Electrochem. Energy Rev. 3 (2) (2020) 271–285, https://doi.org/10.1007/s41918-020-00063-6.
[19] M.W. Ahmad, S. Anand, B. Dey, A. Fatima, D.J. Yang, A. Choudhury, N/P/O/S heteroatom-doped porous carbon nanofiber mats derived from a polyacrylonitrile/l -cysteine/P2O5Precursor for flexible electrochemical supercapacitors, ACS Appl. Energy Mater. 4 (11) (2021) 12177–12190, https://doi.org/10.1021/acsaem.1c01790.
[20] P. Lannelongue, R. Bouchal, E. Mourad, C. Bodin, M. Olarte, S. le Vot, F. Favier, O. Fontaine, "Water-in-salt" for supercapacitors: a compromise between voltage, power density, energy density and stability, J. Electrochem. Soc. 165 (3) (2018) A657–A663, https://doi.org/10.1149/2.0951803jes.
[21] R.-S. Kühnel, D. Reber, C. Battaglia, Perspective—electrochemical stability of water-in-salt electrolytes, J. Electrochem. Soc. 167 (7) (2020), https://doi.org/10.1149/1945-7111/ab7c6f, 070544.
[22] S. Enayat, M.K. Tran, D. Salpekar, M.A. Kabbani, G. Babu, P.M. Ajayan, F. M. Vargas, From crude oil production nuisance to promising energy storage material: development of high-performance asphaltene-derived supercapacitors, Fuel 2020 (263) (September 2019) 116641, https://doi.org/10.1016/j.fuel.2019.116641.
[23] A. Sowmya, S. Meenakshi, A novel quaternized chitosan-melamine-glutaraldehyde resin for the removal of nitrate and phosphate anions, Int. J. Biol. Macromol. 64 (2014) 224–232, https://doi.org/10.1016/j.ijbiomac.2013.11.036.
[24] S. Sembiring, A. Riyanto, R. Situmeang, Z. Sembiring, N. Susanti, I. Firdaus, Effect of amorphous rice husk silica addition on the structure of asphalt composite, J. Met. Mater. Miner. 30 (4) (2020) 113–118, https://doi.org/10.14456/jmmm.2020.59.
[25] L.S. Zaremba, W.H. Smoleński, Optimal portfolio choice under a liability constraint, Ann. Oper. Res. 97 (1–4) (2000) 131–141, https://doi.org/10.1023/A.
[26] N. Afanasjeva, A. González-Córdoba, M. Palencia, Mechanistic approach to thermal production of new materials from asphaltenes of castilla crude oil, Processes 8 (12) (2020) 1–17, https://doi.org/10.3390/pr8121644.
[27] F. Amin, A. Reza, S. Nazar, A study on the adsorption and catalytic oxidation of asphaltene onto nanoparticles, J. Pet. Sci. Technol. 7 (2) (2017) 21–29.
[28] W. Hu, R. Xiang, K. Zhang, Q. Xu, Y. Liu, Y. Jing, J. Zhang, X. Hu, Y. Zheng, Y. Jin, X. Yang, C. Lu, Electrochemical performance of coaxially wet-spun hierarchically porous lignin-based carbon/graphene fiber electrodes for flexible supercapacitors, ACS Appl. Energy Mater. 4 (9) (2021) 9077–9089, https://doi.org/10.1021/acsaem.1c01379.
[29] K. Thileep Kumar, G. Sivagaami Sundari, E. Senthil Kumar, A. Ashwini, M. Ramya, P. Varsha, R. Kalaivani, M. Shanmugaraj Andikkadu, V. Kumaran, R. Gnanamuthu, S.Z. Karazhanov, S. Raghu, Synthesis of nanoporous carbon with new activating agent for high-performance supercapacitor, Mater. Lett. 218 (2018) 181–184, https://doi.org/10.1016/j.matlet.2018.02.017.
[30] Z. Li, X. Gao, L. Wu, K. Wang, N. Kobayashi, Preparation of activated carbons from poplar wood by chemical activation with KOH, J. Porous. Mater. 24 (1) (2017) 193–202, https://doi.org/10.1007/s10934-016-0252-6.
[31] R. Lopez, Adsorción En Sólidos Mesoporosos, Univ. Nac. San Luis. Argentina (**2004**) 19–51. *Capitulo 3*.
[32] K.S.W. Sing, R.T. Williams, Physisorption hysteresis loops and the characterization of nanoporous materials, Adsorpt. Sci. Technol. 22 (10) (2004) 773–782, https://doi.org/10.1260/0263617053499032.
[33] A.V. Neimark, Y. Lin, P.I. Ravikovitch, M. Thommes, Quenched solid density functional theory and pore size analysis of micro-mesoporous carbons, Carbon N. Y. 47 (7) (2009) 1617–1628, https://doi.org/10.1016/J.CARBON.2009.01.050.
[34] L. Wu, Y. Li, Z. Fu, B.-L. Su, Hierarchically structured porous materials: synthesis strategies and applications in energy storage | enhanced reader, Natl. Sci. Rev. 7 (11) (2020) 1667–1701, https://doi.org/10.1093/nsr/nwaa183.
[35] R. Muzyka, S. Drewniak, T. Pustelny, M. Chrubasik, G. Gryglewicz, Characterization of graphite oxide and reduced graphene oxide obtained from different graphite precursors and oxidized by different methods using Raman spectroscopy, Materials (Basel) 11 (7) (2018), https://doi.org/10.3390/MA11071050.
[36] T. Wang, S. Kumar, Electrospinning of polyacrylonitrile nanofibers, J. Appl. Polym. Sci. 102 (2) (2006) 1023–1029, https://doi.org/10.1002/app.24123.
[37] C.A. Velásquez, F.A. Vásquez, M. Alvarez-Láinez, A. Zapata-González, J. A. Calderón, Carbon nanofibers impregnated with Fe3O4 nanoparticles as a flexible and high capacity negative electrode for lithium-ion batteries, J. Alloys Compd. 862 (2021) 158045, https://doi.org/10.1016/j.jallcom.2020.158045.
[38] X.J. Lee, B.Y.Z. Hiew, K.C. Lai, L.Y. Lee, S. Gan, S. Thangalazhy-Gopakumar, S. Rigby, Review on graphene and its derivatives: synthesis methods and potential industrial implementation, J. Taiwan Inst. Chem. Eng. 98 (2019) 163–180, https://doi.org/10.1016/j.jtice.2018.10.028.
[39] R. Doherty, S. Rezaee, S. Enayat, M. Tavakkoli, F.M. Vargas, in: F.M. Vargas, M. Tavakkoli (Eds.), Asphaltene Deposition, 1st Editio, CRC Press, 2018.
[40] D. Hulicova-Jurcakova, M. Kodama, S. Shiraishi, H. Hatori, Z.H. Zhu, G.Q. Lu, Nitrogen-enriched nonporous carbon electrodes with extraordinary supercapacitance, Adv. Funct. Mater. 19 (11) (2009) 1800–1809, https://doi.org/10.1002/adfm.200801100.
[41] X. Fan, Y. Lu, H. Xu, X. Kong, J. Wang, Reversible redox reaction on the oxygen-containing functional groups of an electrochemically modified graphite electrode for the pseudo-capacitance, J. Mater. Chem. 21 (46) (2011) 18753–18760, https://doi.org/10.1039/c1jm13214h.
[42] M.T. Huynh, C.W. Anson, A.C. Cavell, S.S. Stahl, S. Hammes-Schiffer, Quinone 1 E- and 2 e−/2 H+ reduction potentials: identification and analysis of deviations from systematic scaling relationships, J. Am. Chem. Soc. 138 (49) (2016) 15903–15910, https://doi.org/10.1021/jacs.6b05797.
[43] L. Wang, Y. Zhou, J. Qiu, Influence of pore structures on the electrochemical performance of asphaltene-based ordered mesoporous carbons, Microporous Mesoporous Mater. 174 (2013) 67–73, https://doi.org/10.1016/j.micromeso.2013.02.024.
[44] M.H. Kim, K.B. Kim, S.M. Park, K.C. Roh, Hierarchically structured activated carbon for ultracapacitors, Sci. Rep. 6 (February) (2016) 2–7, https://doi.org/10.1038/srep21182.
[45] M. Mirzaeian, Q. Abbas, M.R.C. Hunt, P. Hall, Pseudocapacitive effect of carbons doped with different functional groups as electrode materials for electrochemical capacitors, Energies 13 (21) (2020), https://doi.org/10.3390/en13215577.
[46] H. Wang, R. Fan, J. Miao, J. Deng, Y. Wang, Oxygen groups immobilized on micropores for enhancing the pseudocapacitance, ACS Sustain. Chem. Eng. 7 (13) (2019) 11407–11414, https://doi.org/10.1021/acssuschemeng.9b01201.
[47] A. Ilnicka, M. Skorupska, M. Szkoda, Z. Zarach, P. Kamedulski, W. Zielinski, J. P. Lukaszewicz, Combined effect of nitrogen-doped functional groups and porosity of porous carbons on electrochemical performance of supercapacitors, Sci. Rep. 11 (1) (2021) 1–11, https://doi.org/10.1038/s41598-021-97932-x.
[48] Y. Li, D. Zhang, Y. Zhang, J. He, Y. Wang, K. Wang, Y. Xu, H. Li, Y. Wang, Biomass-derived microporous carbon with large micropore size for high-performance supercapacitors, J. Power Sources 448 (September) (2020) 227396, https://doi.org/10.1016/j.jpowsour.2019.227396.
[49] G. Wang, R. Liang, L. Liu, B. Zhong, Improving the specific capacitance of carbon nanotubes-based supercapacitors by combining introducing functional groups on carbon nanotubes with using redox-active electrolyte, Electrochim. Acta 115 (2014) 183–188, https://doi.org/10.1016/j.electacta.2013.10.165.
[50] Y.J. Oh, J.J. Yoo, Y. Il Kim, J.K. Yoon, H.N. Yoon, J.H. Kim, S. Bin Park, Oxygen functional groups and electrochemical capacitive behavior of incompletely reduced graphene oxides as a thin-film electrode of supercapacitor, Electrochim. Acta 116 (2014) 118–128, https://doi.org/10.1016/j.electacta.2013.11.040.
[51] B. Pal, S. Yang, S. Ramesh, V. Thangadurai, R. Jose, Electrolyte selection for supercapacitive devices: a critical review, Nanoscale Adv. 1 (10) (2019) 3807–3835, https://doi.org/10.1039/c9na00374f.
[52] R.E. Ruther, C.-N. Sun, A. Holliday, S. Cheng, F.M. Delnick, T.A. Zawodzinski, J. Nanda, Stable electrolyte for high voltage electrochemical double-layer capacitors, J. Electrochem. Soc. 164 (2) (2017) A277–A283, https://doi.org/10.1149/2.0951702jes.
[53] I. Shaheen, K.S. Ahmad, C. Zequine, R.K. Gupta, A.G. Thomas, M.A. Malik, S. Iram, Sustainable hydrothermal synthesis of cobalt-nickel nanomaterial for supercapacitor using green stabilizing agents, Int. J. Energy Res. 46 (4) (2022) 4599–4608, https://doi.org/10.1002/er.7452.
[54] X.R. Li, Y.H. Jiang, P.Z. Wang, Y. Mo, W. De Lai, Z.J. Li, R.J. Yu, Y.T. Du, X. R. Zhang, Y. Chen, Effect of the oxygen functional groups of activated carbon on its electrochemical performance for supercapacitors, New Carbon Mater. 35 (3) (2020) 232–243, https://doi.org/10.1016/S1872-5805(20)60487-5.
[55] J. Zhao, A.F. Burke, Review on supercapacitors: technologies and performance evaluation, J. Energy Chem. 59 (2021) 276–291, https://doi.org/10.1016/j.jechem.2020.11.013.
[56] G. Lota, K. Lota, E. Frackowiak, Nanotubes based composites rich in nitrogen for supercapacitor application, Electrochem. Commun. 9 (7) (2007) 1828–1832, https://doi.org/10.1016/j.elecom.2007.04.015.
[57] D.M. Anjos, J.K. McDonough, E. Perre, G.M. Brown, S.H. Overbury, Y. Gogotsi, V. Presser, Pseudocapacitance and performance stability of quinone-coated carbon onions, Nano Energy 2 (5) (2013) 702–712, https://doi.org/10.1016/j.nanoen.2013.08.003.
[58] L. Lin, H. Xie, Y. Lei, R. Li, X. Liu, J. Ou, Nitrogen source-mediated cocoon silk-derived N, O-doped porous carbons for high performance symmetric supercapacitor, J. Mater. Sci. Mater. Electron. 31 (13) (2020) 10825–10835, https://doi.org/10.1007/s10854-020-03634-x.
[59] H. Xu, C. Wu, X. Wei, S. Gao, Hierarchically porous carbon materials with controllable proportion of micropore area by dual-activator synthesis for high-performance supercapacitors, J. Mater. Chem. A 6 (31) (2018) 15340–15347, https://doi.org/10.1039/c8ta04777d.

[60] Y. Kumar, G.P. Pandey, S.A. Hashmi, Gel polymer electrolyte based electrical double layer capacitors: comparative study with multiwalled carbon nanotubes and activated carbon electrodes, J. Phys. Chem. C 116 (50) (2012) 26118–26127, https://doi.org/10.1021/jp305128z.

[61] N.H. Basri, M. Deraman, R. Daik, M.T.M. Ayob, M.I. Sahri, N.S.M. Nor, B.N. M. Dolah, S. Soltaninejad, Electrochemical impedance spectroscopy study of supercapacitors using deposited nickel oxide nanoparticles carbon monolith electrodes, Adv. Mater. Res. 1112 (July) (2015) 236–240, https://doi.org/10.4028/www.scientific.net/amr.1112.236.

[62] B. Hirschorn, M.E. Orazem, B. Tribollet, V. Vivier, I. Frateur, M. Musiani, Determination of effective capacitance and film thickness from constant-phase-element parameters, Electrochim. Acta 55 (21) (2010) 6218–6227, j.electacta.2009.10.065.

[63] G.M. Burke, D.E. Wurster, M.J. Berg, P. Veng-Pedersen, D.D. Schottelius, Surface characterization of activated charcoal by X-ray photoelectron spectroscopy (XPS): correlation with phenobarbital adsorption data, Pharm. Res. Off. J. Am. Assoc. Pharm. Sci. (1992) 126–130, https://doi.org/10.1023/A:1018900431661.

[64] R.J.J. Jansen, H. van Bekkum, XPS of nitrogen-containing functional groups on activated carbon, Carbon N. Y. 33 (8) (1995) 1021–1027, https://doi.org/10.1016/0008-6223(95)00030-H.

[65] A. Malas, A. Bharati, O. Verkinderen, B. Goderis, P. Moldenaers, R. Cardinaels, Effect of the GO reduction method on the dielectric properties, electrical conductivity and crystalline behavior of PEO/RGO nanocomposites, Polymers (Basel) 9 (11) (2017) 10–12, https://doi.org/10.3390/polym9110613.